Article

Stochastic Multi-Objective Optimal Reactive Power Dispatch with the Integration of Wind and Solar Generation

Faraz Bhurt [1], Aamir Ali [1], Muhammad U. Keerio [1], Ghulam Abbas [2], Zahoor Ahmed [3], Noor H. Mugheri [1] and Yun-Su Kim [4],*

[1] Department of Electrical Engineering, Quaid-e-Awam University of Engineering Science and Technology, Nawabshah 67450, Sindh, Pakistan
[2] School of Electrical Engineering, Southeast University, Nanjing 210096, China; lashariabbas@seu.edu.cn
[3] Department of Electrical Engineering, Balochistan University of Engineering and Technology, Khuzdar 89100, Balochistan, Pakistan
[4] Graduate School of Energy Convergence, Gwangju Institute of Science and Technology (GIST), Gwangju 61005, Republic of Korea
* Correspondence: yunsukim@gist.ac.kr

Abstract: The exponential growth of unpredictable renewable power production sources in the power grid results in difficult-to-regulate reactive power. The ultimate goal of optimal reactive power dispatch (ORPD) is to find the optimal voltage level of all the generators, the transformer tap ratio, and the MVAR injection of shunt VAR compensators (SVC). More realistically, the ORPD problem is a nonlinear multi-objective optimization problem. Therefore, in this paper, the multi-objective ORPD problem is formulated and solved considering the simultaneous minimization of the active power loss, voltage deviation, emission, and the operating cost of renewable and thermal generators. Usually, renewable power generators such as wind and solar are uncertain; therefore, Weibull and lognormal probability distribution functions are considered to model wind and solar power, respectively. Due to the unavailability and uncertainty of wind and solar power, appropriate PDFs have been used to generate 1000 scenarios with the help of Monte Carlo simulation techniques. Practically, it is not possible to solve the problem considering all the scenarios. Therefore, the scenario reduction technique based on the distance metric is applied to select the 24 representative scenarios to reduce the size of the problem. Moreover, the efficient non-dominated sorting genetic algorithm II-based bidirectional co-evolutionary algorithm (BiCo), along with the constraint domination principle, is adopted to solve the multi-objective ORPD problem. Furthermore, a modified IEEE standard 30-bus system is employed to show the performance and superiority of the proposed algorithm. Simulation results indicate that the proposed algorithm finds uniformly distributed and near-global final non-dominated solutions compared to the recently available state-of-the-art multi-objective algorithms in the literature.

Keywords: non-dominated sorting genetic algorithm; renewable power sources; optimal reactive power dispatch; probability distribution function

1. Introduction

In power system optimization, reactive power management helps to maintain voltage levels at all buses and reduces system losses. Optimal reactive power dispatch (ORPD) is crucial in enhancing the power system stability, reducing losses, improving reliability, enhancing the active power transfer capability, and enabling non-dispatchable renewable energy generation. ORPD also facilitates efficient operation and effective utilization of power system resources, leading to a more reliable and resilient electrical grid [1]. Reactive power flow is inevitable in power systems due to the prevalence of inductive loads and the consumption of reactive power by components such as transformers and transmission lines [2]. Therefore, generating enough reactive power in a network to meet the needs

of VAR (volt-ampere-reactive) consumers is necessary, while avoiding excessive heat loss and an undesirable voltage drop. In optimal reactive power dispatch (ORDP), the objective is to minimize real power loss in the system, considering that reactive power flow results in actual (active) power loss. In a typical network, adjustments are made to the voltages of generator buses, settings of passive devices such as transformers, and shunt VAR compensators (SVC) to achieve the desired objective. During optimization, certain constraints must be satisfied, including load bus voltage limits, generator reactive power capabilities, line capacities, and power balance. In the literature, the widely considered objective functions to solve ORPD problems are power loss, voltage deviation (VD), and the local stability indicator (L_{index}). These objectives aim to ensure the voltages at consumer terminals are close to the desired level (typically 1 p.u.) while controlling the flow of reactive power [3]. However, achieving this objective does not guarantee the lowest real power loss in the system. It is possible to consider both objectives of minimizing real power loss and voltage deviation together during the optimization process to find a compromise solution. However, these objectives are selected based on the significance placed on specific aspects of the network.

Several research papers have investigated the ORDP problem for power systems incorporating conventional thermal units. These include classical algorithms such as the interior point method [4] and quadratic programming [5]. As discussed, ORPD is a constrained type of problem, and classical algorithms have limitations in effectively incorporating all these constraints, potentially resulting in violated constraints or conservative solutions. ORDP problems involve discrete variables, such as shunt capacitors' switching operations and transformers' tap settings. Classical algorithms may struggle to efficiently handle these discrete variables, leading to suboptimal or infeasible solutions. Classical algorithms may lack robustness in dealing with uncertainties and variations in the power system, such as changes in load demand or the presence of renewable energy sources. They may struggle to adapt and provide optimal solutions under varying operating conditions. To address these limitations, advanced optimization techniques such as evolutionary algorithms, metaheuristic algorithms, and machine learning-based approaches have been proposed to enhance the efficiency, robustness, and scalability of ORDP solutions. These techniques aim to overcome the shortcomings of classical algorithms and provide improved solutions for optimal reactive power dispatch problems. These include modified differential evolution (MDE) [6], the opposition-based gravitational search algorithm (OGSA) [7], continuous ant colony-based differential evolution [8], quasi-oppositional-based learning (QOBE) [9], the oppositional teaching learning-based optimization algorithm [10], moth-flame optimization (MFO) [11], and the improved gravitational search algorithm (IGSA) [12], which were implemented to solve single- and weighted-sum multi-objective ORPD problems. Moreover, to increase the convergence and speed of evolutionary algorithms, their mix flavors, such as hybrid algorithms, are designed to solve ORPD problems. These include hybrid PSO and ICA (PSO-ICA) [13], the hybrid simplex and firefly algorithm (HFA) [14], the hybrid modified imperialist competitive algorithm, and invasive weed optimization (MICA-IWO) [15], which were implemented to solve ORPD problems.

As discussed, ORPDs are multi-objective problems. The single-objective EA has the limitation of a lack of trade-off between various conflicting objective functions and is limited in decision-making because of the single non-dominated solution. To overcome the limitations of single-objective EAs, multi-objective evolutionary algorithms have been developed. These algorithms efficiently find many final non-dominated solutions of conflicting objective functions in a single simulation run, allowing decision-makers to explore trade-offs and select the most suitable solution based on their preferences. The non-dominated sorting genetic algorithm II (NSGAII) [16], improved generalized DE (I-GDE3) [17], two-archive multi-objective Grey wolf optimizer (2ArchMGWO) [18], classification and Pareto domination-based MOEA (CPSMOEA) [19], modified NSGAII (MNSGAII) [20], hybrid fuzzy MOEA (HFMOEA) [21], multi-objective chaotic improved PSO (MOCIPSO) [22], classification and Pareto domination-based MOEA (CPDMOEA) [19], multi-objective DE

(MODE) [23], chaotic parallel vector evaluated interactive honey bee mating optimization (CPVEIHBMO) [24], multi-objective ant lion optimization (MOALO) [25], multi-objective imperialist competitive algorithm (MOICA) [26], and the strength Pareto multi-group search optimizer (SPMGSO) [27] were applied to solve MOORPD problems considering conventional thermal generators.

Renewable energy sources such as wind and solar power have grown in popularity recently and present a challenge for the ORPD problem. Incorporating the uncertainty of wind and solar generation has been achieved through the use of optimization techniques such as the general algebraic modeling system (GAMS) [28,29], hybrid artificial physics optimization (APO) and PSO, called APO-PSO [30], NSGAII [31], hybrid modified NSGAII and TOPSIS [32], the enhanced firefly algorithm (EFA) [33], the opposition-based self-adaptive modified gravitational search algorithm (OSAMGSA) [34], hybrid NSGAII and differential evolution for multi-objective (DEMO) [35], and the two-point estimate method (TPEM) [36]. These papers mainly consider two objective functions, from power loss, cost, emission, and voltage deviation, to solve the ORPD problem.

Furthermore, recently, a large number of many-objective evolutionary algorithms (MaOEAs) were designed to solve mathematical optimization problems considering more than three objective functions. Optimizing more than three objectives can become increasingly complex as the number of objectives increases. The use of many-objective evolutionary algorithms (MaOEAs) is indeed a relevant approach to effectively address this challenge. The MaOEAs include NSGAIII [37], the knee-point-driven evolutionary algorithm (KnEA) [38], the improved decomposition-based evolutionary algorithm (ID-BEA) [39], the inverted generational distance (IGD)-based MaOEA (MaOEAIGD) [40], a MaOEA based on an independent two-stage approach (MaOEAIT) [41], and a MaOEA based on objective space reduction and diversity improvement (MaOEARD) [42]. These algorithms are specifically designed to handle a large number of objectives (specially more than three) and can provide more robust solutions in such cases. Recently, an ORPD-based MaOP has been formulated in [43] considering four objective functions (minimization of cost and emissions, and maximization of the transmission line power factor and the voltage stability index), simultaneously optimized using NSGAIII.

To the best of the authors' knowledge, no existing literature has attempted to address the stochastic ORPD problem involving unpredictable load demand, wind, and solar power (specifically, photovoltaic or PV) subject to simultaneously minimizing three or four objective functions. PV systems are becoming increasingly crucial in smart grids due to the abundant, affordable, and widely available solar energy they harness. Consequently, it is essential to incorporate ORPD analysis considering both solar and wind power. However, incorporating multiple renewable sources into the optimal power distribution problem increases the complexity. In addition to the variability in the load demand, the uncertainty associated with renewable sources must also be considered. The stochastic ORPD problem can be conceptualized as a multi-objective optimization problem incorporating wind and solar power, uncertain load demand, and other relevant variables.

This research utilizes a scenario-based approach to formulate and solve a single-objective ORPD problem that considers the stochastic characteristics of load demand, wind speed, and solar irradiance. The main focus of the study revolves around the multi-objective optimization aspect. The modified IEEE 30-bus test system is optimized simultaneously for various objectives, including real power loss, aggregate voltage deviation at load buses, the active power supply cost, and emissions. The Gaussian probability distribution function (PDF) is the most suitable model to represent the uncertainty in load demand. The stochastic behavior of wind speed is simulated using the Weibull PDF, while the lognormal PDF captures the stochastic nature of solar PV. A Monte Carlo simulation is conducted to generate many alternative scenarios for each of these uncertain variables. Subsequently, a scenario reduction technique is applied to select a specific number of representative situations from the generated alternatives. By lowering the proposed problem's complexity while keeping the solution's quality, scenario reduction approaches are considered to

improve the computing efficiency, guarantee a representative sample of scenarios, enable trade-off analysis, and facilitate decision-making.

The selected representative scenarios are implemented to formulate scenario-based ORPD problems and optimized through a new constrained, efficient non-dominated sorting-based bidirectional co-evolutionary algorithm (BiCo) that was not yet tested to solve multi-objective scenario-based ORPD problems. The proposed algorithm is applied to solve scenario-based ORPD problems. The critical contributions of this work are outlined as follows:

- Formulation of a deterministic and stochastic ORPD problem incorporating uncertain load demand, wind, and solar power in a modified IEEE 30-bus test system.
- Generation of numerous scenarios for uncertain demand and renewable energy applying the Monte Carlo method and selection of representative scenarios using a backward reduction algorithm of scenario reduction.
- A new efficient NSGAII-based bidirectional co-evolutionary algorithm with an integrating constraint-handling technique is applied to solve the multi/many-objective ORPD problem, that simultaneously considers 2, 3, and 4 objective functions.
- A comparative study of the deterministic and stochastic multi-objective ORPD for base configurations of IEEE 30 and the modified IEEE 30-bus test system.
- Detailed analyses and comparisons of the proposed scenarios considering all the constraints in deterministic and stochastic multi-objective ORPD problems.

This paper is structured as follows: Section 2 provides the problem formulation, while Section 3 presents a detailed explanation of scenario generation and reduction using MCS. The implementation of the proposed algorithm to the multi-objective ORPD problem is demonstrated in Section 4. The simulation results are presented in Section 5, followed by discussions of all the study cases in Section 6. Finally, the research conclusions are presented in Section 7.

2. Problem Formulation

Without loss of generality, a constrained multi-objective optimization problem can be given as:

$$
\begin{aligned}
minF(x) &= (f_1(x), f_2(x), f_m(x))^T \\
g_i(x) &\leq 0, i = 1, 2, 3 \ldots, p \\
h_i(x) &= 0, i = 1, 2, 3 \ldots q \\
x &= ((x_1, x_2, ..x_D)^T \in S)
\end{aligned}
\tag{1}
$$

where $F(x)$ consists of vector objective functions, m shows the total number of objective functions, x is the decision vector, $g(x)$ and $h(x)$ are the number of p and q nonlinear inequality and equality constraints, respectively, and D is the number of dimensions in the decision vector. The decision vector of the proposed problem is:

$$
x = \left[\underbrace{V_{G,1}, \cdots, V_{G,N_g}}_{V_G}, \underbrace{Q_{c,1}, Q_{c,NC}}_{Q_c}, \underbrace{T_{k,1}, T_{k,NT}}_{T_k} \right]^T
\tag{2}
$$

This study considers four objective functions to solve the ORPD problem. These include the expected cost of active and reactive power injection (C) in (USD/h), the expected emission rate (E) in tons per hour (t/h), the expected power loss (P_L) in MW, and the expected voltage deviation (VD) in p.u. Functional loss is one of the most predominant objective functions in the ORPD problem that leads to an improved system efficiency, enhanced voltage stability, economic benefits for power utilities, and better integration of renewable energy sources. It promotes the optimal use of resources, cost savings, and a

more sustainable power system. Therefore, the first objective function f_1 is the expected minimization of power loss, and it is computed as:

$$f_1 = \sum_{sc=1}^{n_{sc}} \tau_{sc} \sum_{k=1}^{nl} G_k[V_i^2 + V_j^2 - 2V_iV_j\cos(\delta_{ij})] \qquad (3)$$

where G_k is the shunt conductance of the kth line between bus i and j and $\delta_{ij} = \delta_i - \delta_j$ is the branch voltage angle. Considering power loss minimization results in an increase in the system voltage beyond a specific limit. Therefore, to control the voltage level near unity, it is desirable to consider voltage deviation (VD) as the objective function to ensure better voltage regulation, improve system security, safeguard electrical equipment, reduce equipment failures, optimize power flow, and enhance the overall system efficiency. The second objective function f_2 is the expected VD, and mathematically, it is calculated as:

$$f_2 = \sum_{sc=1}^{n_{sc}} \tau_{sc} \left(\sum_{p=1}^{N_{pq}} |V_{L_p} - 1| \right) \qquad (4)$$

where, N_{pq} shows the total number of load buses and V_{L_p} is the PQ bus voltage. The optimization of power generation, voltage stability, grid dependability, and the efficient integration of renewable energy sources are made possible by including active and reactive power costs in formulating the ORPD problem. This leads to an enhanced system performance and cost-effectiveness. Therefore, the third objective function f_3 is the expected cost of active and reactive power generation, and it is calculated as follows:

$$f_3 = \sum_{sc=1}^{n_{sc}} \tau_{sc} \sum_{i=1}^{N_T} (C_i(P_{gT}) + C_i(Q_{gT})) + \sum_{sc=1}^{n_{sc}} \tau_{sc} \sum_{j=1}^{N_W} C_j(P_{gW}) + \sum_{sc=1}^{n_{sc}} \tau_{sc} \sum_{k=1}^{N_S} C_k(P_{gS}) \qquad (5)$$

where, f_3 is the expected cost of the power supply, τ_{sc} is the probability of scenario sc, N_{sc} is the total number of scenarios, N_T, N_W, and N_s are the total numbers of thermal, wind, and solar PV generators, respectively, and $C_i(P_{gT})$ is the quadratic cost of the ith thermal generator, which can be given as:

$$\begin{aligned} C_i(P_{gT}) &= a_i + b_iP_{gT_i} + c_iP_{gT_i}^2 \\ C_i(Q_{gT}) &= a_i + b_iQ_{gT_i} + c_iQ_{gT_i}^2 \end{aligned} \qquad (6)$$

In this work, the cost parameters a_i, b_i, and c_i are the same for the active and reactive power generation, and these cost coefficients are shown in Table 1. The generator at bus 1 is the reference bus, and generators installed at buses 2, 11, and 13 are the voltage-controlled generators. In Equation (5), $C_j(P_{gW})$ and $C_k(P_{gS})$ are the costs of wind and solar PV generators. In this work, the wind and solar PV generators considered linear cost functions, whose parameters C_j and C_k were set to 2.03 USD/MWh.

Table 1. Cost and emission parameters.

Bus #	a	b	c	α	β	γ	ω	μ
1	0	2	0.00375	0.04091	−0.05554	0.0649	0.0002	2.857
2	0	1.75	0.0175	0.02543	−0.06047	0.05638	0.0005	3.333
11	0	3	0.025	0.04258	−0.05094	0.04586	1.00×10^{-6}	8
13	0	3	0.025	0.06131	−0.05555	0.05151	1.00×10^{-5}	6.667

The emission rate is one of the objective functions in ORPD problems that promotes environmental sustainability, encourages renewable integration, improves system efficiency,

and meets stakeholder expectations for cleaner and more sustainable power systems. Therefore, the fourth objective function f_4 in this study is the emission rate [44], computed as:

$$f_4 = \sum_{sc=1}^{n_{sc}} \tau_{sc} \sum_{i=1}^{N_{TG}} \left[\left(\alpha_i + \beta_i P_{gT_i} + \gamma_i P_{gT_i}^2 \right) + \omega_i \exp\left(\mu_i P_{gT_i} \right) \right] \quad (7)$$

where, $\alpha_i, \beta_i, \gamma_i, \omega_i$, and μ_i are the emission coefficients associated with the ith thermal generator, which are provided in Table 1. The equality constraints, $h_i(x)$, given in Equation (1) can be defined as:

$$P_{G_i} - P_{D_i} = V_i \sum_{j=1}^{N_b} V_j \left[G_{ij} \cos\left(\delta_{ij} \right) - B_{ij} \sin\left(\delta_{ij} \right) \right]$$
$$Q_{G_i} - Q_{D_i} = V_i \sum_{j=1}^{N_b} V_j \left[G_{ij} \sin\left(\delta_{ij} \right) - B_{ij} \cos\left(\delta_{ij} \right) \right] \quad (8)$$

where B_{ij} is the susceptance of a line between bus i and j and P_{D_i} and Q_{D_i} are the fundamental and reactive power demands. The number of inequality constraints, $g_i(x)$, is given as:

- Generator constraints:

$$V_{G_i}^{\min} \leq V_{G_i} \leq V_{G_i}^{\max} \forall i \in N_G \quad Q_{G_i}^{\min} \leq Q_{G_i} \leq Q_{G_i}^{\max} \forall i \in N_G \quad (9)$$

- Transformer constraints:

$$Tap_m^{\min} \leq Tap_m \leq Tap_m^{\max} \forall m \in N_{TX} \quad (10)$$

- Shunt compensator constraints:

$$Q_{c_k}^{\min} \leq Q_{C_k} \leq Q_{C_k}^{\max} \forall k \in NC \quad (11)$$

- Security constraints:

$$V_L^{min} \leq V_L \leq V_L^{max} \forall L \in N_L \quad (12)$$

$$S_l \leq S_l^{max} \forall l \in nl \quad (13)$$

Most multi-objective evolutionary algorithms (MOEAs) examined in the literature review use one typical method for handling constraints, known as the penalty function approach, which manages constraint violations by applying a penalty parameter. Inappropriately selecting penalty parameters can also result in an infeasible solution. Consequently, when dealing with a realistic multi-objective problem with constraints, selecting an appropriate constraint-handling technique to guide the MOEAs is crucial. This helps search the entire feasible space, escape the infeasible region, and find a widely distributed Pareto front close to the global optimum. Therefore, in this paper, the constraint domination principle [45] was implemented to handle constraints in the proposed bidirectional co-evolutionary algorithm.

Furthermore, base case loading, called deterministic ORPD, was conducted using the base configurations of the IEEE 30 system, that consists of conventional thermal generators only to manage the load demand. The results obtained from this case were compared to previously published findings. For the stochastic multi-objective ORPD analysis, the IEEE 30-bus system was modified to incorporate a wind turbine at bus 5 and a solar PV generation at bus 8. The parameters of the systems studied in this research are summarized in Table 2.

Table 2. Summary of the proposed IEEE 30-bus test system under study.

Items	Deterministic (IEEE 30-Bus Base Configuration)			Stochastic Scenario (IEEE 30-Bus Modified Configuration)	
Name	**Quantity**	**Explanation**		**Quantity**	**Explanation**
Buses	30	[46]		720	24 scenarios, and in each scenario, 30 buses. Total $N_b \times n_{sc}$ buses.
N_g	6	Buses: 1 (ref), 2, 5, 8, 11, 13		96	24 scenarios, and in each scenario, 4 thermal generators. Total $N_T \times n_{sc}$ thermal generators.
N_w	--	--		24	24 scenarios, and in each scenario, 1 wind generator. Total $N_W \times n_{sc}$ wind generators.

Table 2. *Cont.*

Items	Deterministic (IEEE 30-Bus Base Configuration)			Stochastic Scenario (IEEE 30-Bus Modified Configuration)	
Name	**Quantity**	**Explanation**		**Quantity**	**Explanation**
N_s	--	--		24	24 scenarios, and in each scenario, 1 solar PV unit. Total $N_s \times n_{sc}$ solar PV units.
Q_c	9	Buses: 10, 12, 15, 17, 20, 21, 23, 24, 29		216	24 scenarios, and in each scenario, 9 SVCs. Total $N_{SVC} \times n_{sc}$ SVCs.
Tap	4	Branches: 11, 12, 15, 36		96	24 scenarios, and in each scenario, 4 transformers. Total $N_{TX} \times n_{sc}$ transformers.
D	19	6 for V_G, 9 for SVC, and 4 for TX		456	6×24 for V_G, 9×24 for SVC, and 4*24 for TX.
N_{pq}	24	[0.95, 1.05] p.u.		576	24×24 closed to [0.95, 1.05] p.u.

3. MCA-Based Scenario Generation and Reduction Technique

This section focuses on the modified IEEE 30-bus system incorporating uncertain non-dispatchable generation and load demand. The original scenario assumes a fully loaded (fixed) network, while the modified network considers the unpredictability of demand. This section addresses the modeling of uncertainty in load demand and renewable energy sources, as well as the approaches for scenario generation and reduction.

Scenario Generation of Wind, Solar, and Load Uncertainties

A normal PDF with a known mean (μ_d) and standard deviation (σ_d) was used to describe load uncertainty as in [29], and mathematically, P_d, computed as:

$$\Delta_D(P_D) = \frac{1}{\sigma_D \sqrt{2\pi}} \exp\left[-\frac{(P_D - \mu_D)^2}{2\sigma_D^2}\right] \tag{14}$$

In the literature, Weibull PDF has been applied to generate wind velocity, v_w, as:

$$\Delta_v(v_w) = \left(\frac{\beta}{\alpha}\right)\left(\frac{v_w}{\alpha}\right)^{\beta-1} \exp\left[-\left(\frac{v_w}{\alpha}\right)^{\beta}\right] \tag{15}$$

where α and β are the scale and shape parameters of Weibull PDF. The probability density function (PDF) for the solar irradiance was generated using the lognormal distribution function. Similar to Gaussian and Weibull PDF, the lognormal function also has two parameters, such as mean (μ_s) and standard deviation (σ_s), and is given as:

$$\Delta_G(G_s) = \frac{1}{G_s \sigma_s \sqrt{2\pi}} \exp\left[-\frac{(\ln G_s - \mu_s)^2}{2\sigma^2}\right], \, for \, all \, G_s > 0 \tag{16}$$

Moreover, the 1000 MCS-based scenarios were generated using Equations (13)–(15) [47,48]. Figures 1–3 represent the 1000 MCS scenarios of probabilistic load demand, wind velocity, and solar irradiances.
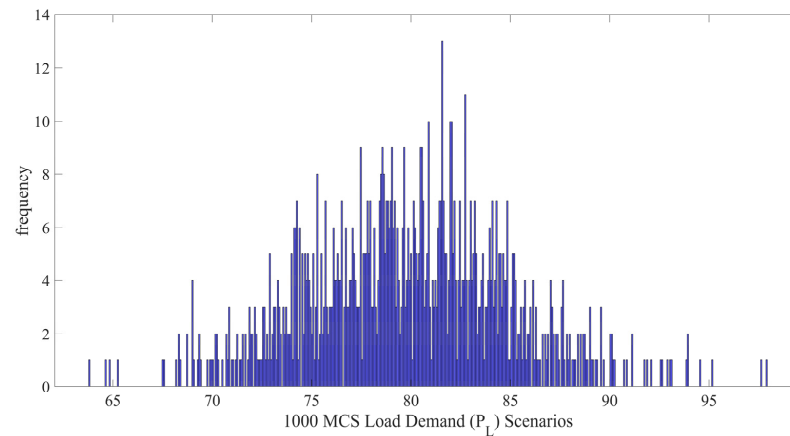
Figure 1. The 1000 Monte Carlo scenarios of load demand.

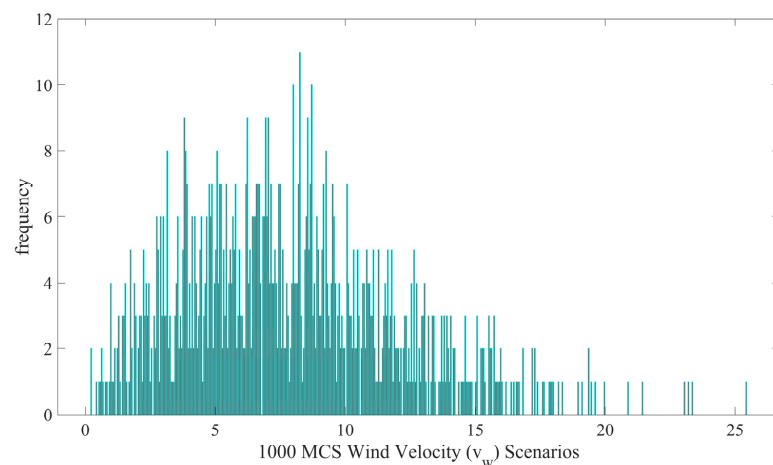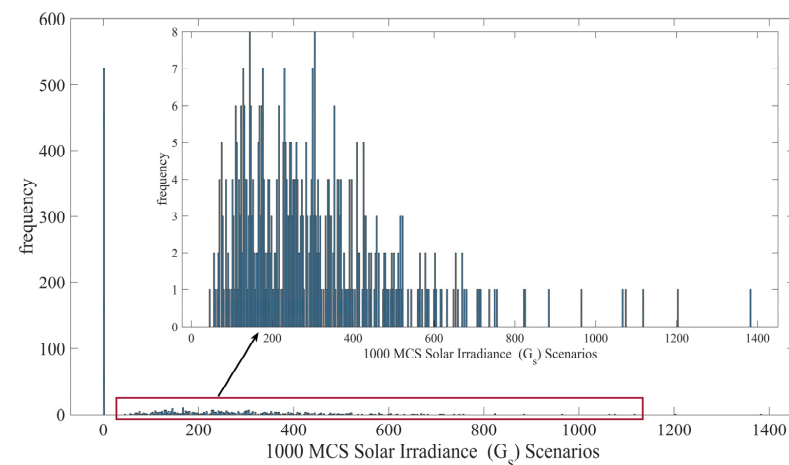**Figure 2.** The 1000 Monte Carlo scenarios of wind velocity.

Figure 3. The 1000 Monte Carlo scenarios of solar irradiances.

It is essential to consider that solar irradiance accounts only if daylight is available. Typically, there would be no solar irradiance during nighttime hours as the sun is not visible. The probability of zero irradiance is about 50%, while the remaining 50% probability is

utilized to construct solar irradiance scenarios using a lognormal distribution. Suppose all the 1000 scenarios of all the load, solar PV, and wind power generations are considered. Then, the 1000 $\times$ 1000 $\times$ 1000 test system is used to solve the ORPD problem. It is impractical to solve such substantial scenarios.

In order to avoid such limitations of the large number of scenarios, in this work, the scenario reduction technique from [49] was employed to find the 24 representative scenarios. These twenty-four representative scenarios are shown in Table 3. The 24 reduced representatives, as shown in Table 3, are analogs to realistic scenarios. In scenario 4, solar irradiance was zero, and the probability of this scenario was 48%. Moreover, Table 3 shows that wind velocity, v_w, and solar irradiances, G_s, complemented each other, the same as those of realistic scenarios. Then, the reduced scenario-based wind velocity and solar irradiances were employed to find the wind and solar PV power generation using Equations (16) and (17):

$$P_{gW}(v_W) = \begin{cases} 0, \text{ for } v_w < v_{in} \text{ and } v_w > v_{ouT} \\ P_{wr}\left(\frac{v_w - v_{in}}{v_r - v_{in}}\right) \text{ for } v_{in} \leq v \leq v_r \\ P_{wr} \text{ for } v_r < v_w \leq v_{ouf} \end{cases} \tag{17}$$

where v_w, v_{in}, v_r, and v_{out} are the actual, cut-in, rated, and cut-out wind velocities, respectively. It is evident from Equation (16) that the power generated by a wind turbine is a piecewise function of the wind speeds. At a given value of solar irradiances (G_s), solar PV power (P_{gS}) can be computed as:

$$P_{gS} = \begin{cases} P_{gr}\left(\frac{G_s^2}{G_{std}R_c}\right) \text{ for } 0 < G_s < R_c \\ P_{gr}\left(\frac{G_s}{G_{std}}\right) \text{ for } G_s \geq R_c \end{cases} \tag{18}$$

where G_{std} is the standard irradiances that are 1000 W/m^2, and R_c is the certain irradiances. In this paper, Equations (16) and (17) were used to compute the maximum generated power of wind and solar PV units, as shown in the fourth and sixth columns of Table 3.

Table 3. Representative reduced scenarios for the proposed study.

sc	%P_D	v_w (m/s)	P_{gW} (MW)	G_s (W/m^2)	P_{gS} (MW)	τ_{sc}
1	0.7422	7.186491	24.2	168.8376	8.4	0.133
2	0.742879	4.911892	11.0	518.0684	25.9	0.021
3	0.748158	16.48807	75.0	824.5378	41.2	0.002
4	0.753088	7.970617	28.7	0	0.0	0.483
5	0.757703	5.061396	11.9	1065.229	50.0	0.002
6	0.767313	6.978557	23.0	67.84026	1.9	0.027
7	0.779955	6.996888	23.1	286.5982	14.3	0.063
8	0.785862	15.73316	73.5	367.6753	18.4	0.004
9	0.791875	15.38266	71.4	170.1946	8.5	0.012
10	0.800161	17.27174	75.0	0	0.0	0.041
11	0.803226	7.533151	26.2	456.7534	22.8	0.017
12	0.80331	7.265045	24.6	604.0629	30.2	0.016
13	0.804655	5.378946	13.7	414.7496	20.7	0.031
14	0.806851	9.527802	37.7	1117.755	50.0	0.001
15	0.809013	8.03871	29.1	353.7884	17.7	0.04
16	0.809959	8.020577	29.0	669.1153	33.5	0.012
17	0.815799	3.257964	1.5	963.8287	48.2	0.001
18	0.818281	8.446844	31.4	755.8481	37.8	0.004
19	0.820037	1.726469	0.0	1202.215	50.0	0.001
20	0.820092	13.72574	61.9	1383.797	50.0	0.001
21	0.829893	9.503078	37.5	884.0359	44.2	0.001
22	0.832635	15.61855	72.8	431.5377	21.6	0.004
23	0.836379	8.56853	32.1	241.3457	12.1	0.072
24	0.89722	16.19869	75.0	253.2671	12.7	0.011

4. Constraint-Handling Technique and MOEAs

MOEAs are popular and powerful tools for solving multi-objective ORPD problems and have successfully found valuable solutions [4,8,11]. Addressing these limitations often involves algorithmic enhancements, problem-specific adaptations, and careful selection of algorithm configurations to ensure the best possible performance. The proposed multi-objective ORPD problem is a realistic, constrained, scenario-based, large-scale optimization problem, as shown in Table 2. For the solution of multi-objective ORPD problems, MOEAs prematurely converge into the local Pareto front (PF), and a subset of the Pareto optimal solution, called the Pareto set (PS), and they fail to explore other promising regions of the search space. In order to resolve these problems, this paper exercised a new bidirectional co-evolutionary (BiCo) constrained MOEA [50] with the integration of the constraint domination principle (CDP) [45] to handle constraints. The constraint technique usually deletes infeasible solutions and accepts feasible solutions. A feasible area is where all decision vectors' degree of constraint violation (CV) is zero. The Pareto front (PF) represents the collection of all Pareto optimal solutions in the objective space. Pareto optimal solutions (PS) encompass all solutions within feasible regions. From the two solutions, e.g., x_u and x_v, x_u are non-dominated solutions if in the objective space, the value of $f(x_u)$ is less than or equal to the value of $f(x_v)$, but for at least one objective function j, $f_j(x_u)$ is less than $f_j(x_v)$. The constraint domination principle is defined as follows.

Based on the two aforementioned definitions, namely feasible and non-domination solutions, the principle of constraint domination was employed to compare two randomly selected populations, e.g., x_u and x_v, where x_u survives in the current iteration and goes to the next iteration if, and only if:

- Both solutions are infeasible, and $CV\left(\vec{x}_u\right) < CV\left(\vec{x}_v\right)$.
- $\vec{x}_u$ is feasible and $\vec{x}_v$ is infeasible.
- Both solutions are feasible, then $f_i\left(\vec{x}_u\right) \le f_i\left(\vec{x}_v\right)$.

The proposed algorithm was elucidated into four steps with the integration of CHT, such as CDP. In the first step, the initial population (P_t) of size N_p was randomly generated considering the upper and lower bounds of the decision vector and the empty archive population (A_t). In the second step, a binary tournament selection scheme was applied to select multiple copies of the best solutions from the ($P_t U A_t$) to generate an offspring population, Q_t, using a simulated binary crossover operator [51]. In the third step, the main population was updated (P_{t+1}) by combining the main, P_t, and offspring, Q_t, populations to generate fronts of non-dominated solutions. In the fourth step, the archive population was updated for the next iteration, A_{t+1}, which is responsible for generating non-dominated infeasible solutions to improve the diversity of the Pareto front [50]. A detailed description of the steps of the proposed algorithms' flow diagram is shown in Figure 4.

5. Simulation Results and Discussion

In this work, the first base case IEEE 30-bus test system, called the deterministic system, without any modifications such as wind and solar integration and operating at base load, was utilized to compare the proposed algorithm with a recently implemented one. The objective functions considered for the comparison were voltage deviation and power loss, commonly used in the literature, aiming to validate and demonstrate the superiority of the proposed algorithm. The single-line diagram of the proposed test network is shown in Figure 5.
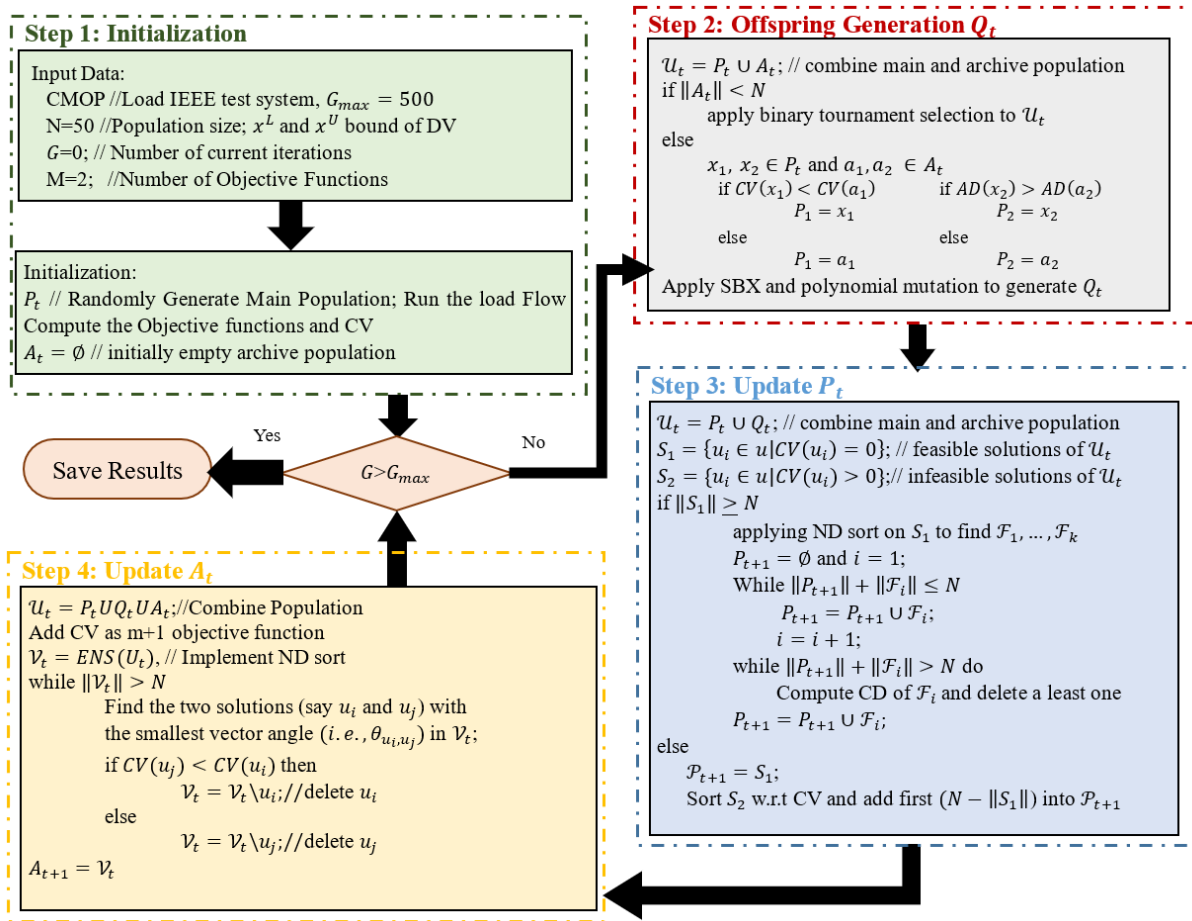
Step 1: Initialization

Input Data:
CMOP //Load IEEE test system, $G_{max} = 500$
N=50 //Population size; x^L and x^U bound of DV
G=0; // Number of current iterations
M=2; //Number of Objective Functions

Initialization:
P_t // Randomly Generate Main Population; Run the load Flow
Compute the Objective functions and CV
$A_t = \emptyset$ // initially empty archive population

Step 2: Offspring Generation Q_t

$\mathcal{U}_t = P_t \cup A_t$; // combine main and archive population
if $\|A_t\| < N$
　　apply binary tournament selection to $\mathcal{U}_t$
else
　　$x_1, x_2 \in P_t$ and $a_1, a_2 \in A_t$
　　if $CV(x_1) < CV(a_1)$　　　if $AD(x_2) > AD(a_2)$
　　　　$P_1 = x_1$　　　　　　　　$P_2 = x_2$
　　else　　　　　　　　　　else
　　　　$P_1 = a_1$　　　　　　　　$P_2 = a_2$
Apply SBX and polynomial mutation to generate Q_t

Step 3: Update P_t

$\mathcal{U}_t = P_t \cup Q_t$; // combine main and archive population
$S_1 = \{u_i \in u | CV(u_i) = 0\}$; // feasible solutions of $\mathcal{U}_t$
$S_2 = \{u_i \in u | CV(u_i) > 0\}$;// infeasible solutions of $\mathcal{U}_t$
if $\|S_1\| \geq N$
　　applying ND sort on S_1 to find $\mathcal{F}_1, \dots, \mathcal{F}_k$
　　$P_{t+1} = \emptyset$ and $i = 1$;
　　While $\|P_{t+1}\| + \|\mathcal{F}_i\| \leq N$
　　　　$P_{t+1} = P_{t+1} \cup \mathcal{F}_i$;
　　　　$i = i + 1$;
　　while $\|P_{t+1}\| + \|\mathcal{F}_i\| > N$ do
　　　　Compute CD of $\mathcal{F}_i$ and delete a least one
　　$P_{t+1} = P_{t+1} \cup \mathcal{F}_i$;
else
　　$\mathcal{P}_{t+1} = S_1$;
　　Sort S_2 w.r.t CV and add first $(N - \|S_1\|)$ into $\mathcal{P}_{t+1}$

Save Results

Yes　　　　$G > G_{max}$　　　　No

Step 4: Update A_t

$\mathcal{U}_t = P_t \cup Q_t \cup A_t$;//Combine Population
Add CV as m+1 objective function
$\mathcal{V}_t = ENS(\mathcal{U}_t)$, // Implement ND sort
while $\|\mathcal{V}_t\| > N$
　　Find the two solutions (say u_i and u_j) with
　　the smallest vector angle (i.e., θ_{u_i,u_j}) in $\mathcal{V}_t$;
　　if $CV(u_j) < CV(u_i)$ then
　　　　$\mathcal{V}_t = \mathcal{V}_t \backslash u_i$;//delete u_i
　　else
　　　　$\mathcal{V}_t = \mathcal{V}_t \backslash u_j$;//delete u_j
$A_{t+1} = \mathcal{V}_t$

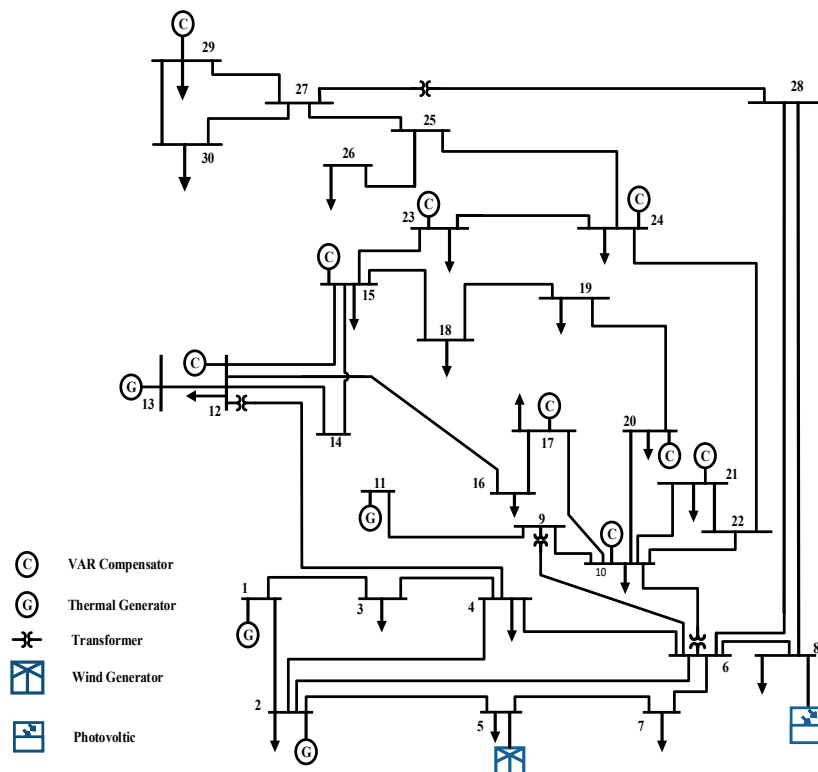**Figure 4.** Flow chart of the proposed algorithm.

Figure 5. Modified IEEE 30-bus test system.

5.1. Deterministic Base Case Multi-Objective ORPD

In this section, state-of-the-art MOEs are implemented to solve multi-objective ORPD problems. To show the superiority and performance of the proposed algorithm in terms of exploration and exploitation compared to the recent algorithms, two popularly used objective functions, power loss and voltage deviation, were considered. The main objective of MOEAs is to generate high-quality solutions that are non-dominated. The quality assessment of non-dominated (ND) solutions involves three key goals: convergence, diversity, and spread. Researchers have extensively evaluated the quality of solution sets obtained by MOEAs, which underscores the need for enhancing the convergence, diversity, and dissemination of the MOEAs' ultimate non-dominated solutions. In the past, various performance metrics have been proposed to facilitate a precise comparison of MOEAs. The most famous performance metric for comparing MOEAs is the hypervolume indicator (HVI) (for details, see [52]). The HVI measures the performance of MOEAs in both convergence and spread; the higher the value of the HVI, the better the final non-dominated solutions. For the statistical results, each algorithm was independently run twenty times to find the best, worst, standard deviation, and HVI values. A larger HVI value indicates better convergence and distribution of PF. More recent algorithms, such as NSGAII [45], ToP [53], CCMO [54], C3M [55], CMME [56], and CMOCSO [57], were implemented to solve the multi-objective deterministic ORPD problems. The simulation results based on the statistics of the HVI (mean, best, worst, and standard deviation values of HVI over ten independent runs) are summarized in Table 4. The last column, %FR, shows the feasibility ratio. It is worthwhile to mention that no constraint violation was observed in any trial run of any algorithm. All experiments in this article were conducted on the platform developed by Tian et al. (PlatEMO) [58].

Table 4. Statistical comparisons of state-of-the-art MOEAs of all 20 independent runs based on the HVI.

Algorithm	Best	Worst	SD	%FR	BCS	
					f_1	f_2
NSGAII [45]	1.96×10^{-1}	1.92×10^{-1}	1.95×10^{-1}	100	4.576	0.306
ToP [53]	1.94×10^{-1}	1.75×10^{-1}	1.84×10^{-1}	100	4.579	0.301
CCMO [54]	1.94×10^{-1}	1.92×10^{-1}	1.96×10^{-1}	100	4.587	0.293
C3M [55]	1.95×10^{-1}	1.91×10^{-1}	1.93×10^{-1}	100	4.610	0.269
CMME [56]	1.88×10^{-1}	1.83×10^{-1}	1.86×10^{-1}	100	4.602	0.274
CMOCSO [57]	1.94×10^{-1}	1.90×10^{-1}	1.93×10^{-1}	100	4.842	0.125
Proposed	1.97×10^{-1}	1.94×10^{-1}	1.93×10^{-1}	100	4.551	0.325

The simulation results of statistical performance showed that the proposed algorithm found consistent results across all the runs compared to the other algorithms. Out of twenty PFs, each algorithm's best Pareto front (PF) was found using the statistical results shown in Table 4. Figure 6 compares the best PF of all the algorithms with the proposed algorithm. The PF of the proposed algorithm outperformed all others in terms of the first objective function f_1, whereas, for objective function f_2, CMOCSO [57] showed the best result. The decision-maker can take a solution from the population-based, non-dominated solutions. This paper applied the fuzzy weight technique [35] to extract the best compromise solution (BCS) from the best PF of the final non-dominated solutions. In this technique, the first step is to compute the membership function by normalizing the objective function, as:

$$\mu_m^k = \begin{cases} 1 & for\ f_m^k \leq f_m^{min} \\ \frac{f_m^{max} - f_m^k}{f_m^{max} - f_m^{min}} & for\ f_m^{min} < f_m^k < f_m^{max} \\ 0 & for\ f_m^k \geq f_m^{max} \end{cases} \qquad (19)$$
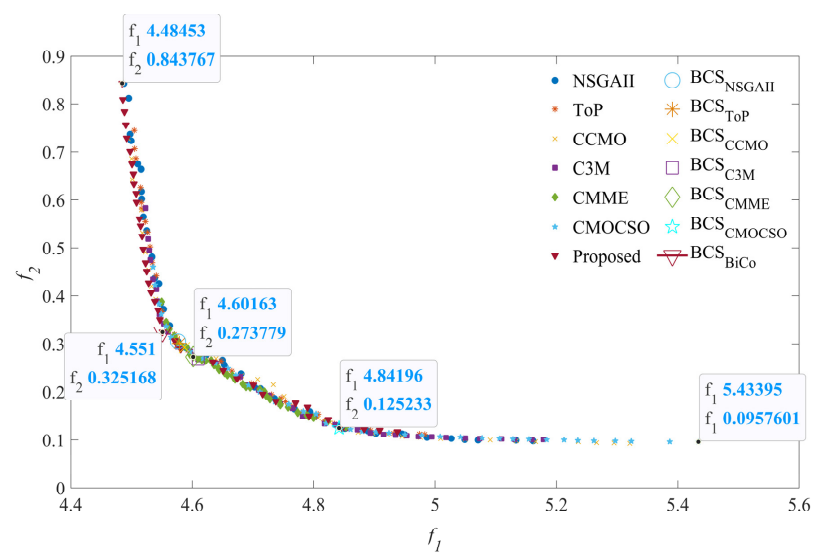
Figure 6. Pareto fronts (PF) of the base case.

Then, each membership function is normalized as:

$$\mu^k = \frac{\Sigma_{m=1}^{M} \mu_m^k}{\Sigma_{k=1}^{N_d} \Sigma_{m=1}^{M} \mu_m^k} \qquad (20)$$

The better consensus solution is the highest value of μ^k out of all non-dominated (Nd) solutions. Figure 6 displays the final non-dominated solutions of all iterations for analysis case 1. Furthermore, Table 5 shows the best compromise solution's decision vector and objective functions. Table 5 demonstrates that all decision variables were within their respective upper and lower bounds, and the MVAr injected by all the generators adhered to the specified limits. Additionally, we compared the simulation results of the base case with an existing method from the literature for solving single- and multi-objective ORPD problems, as shown in Table 6.

Table 5. Simulation results of the base case study case.

Parameters	Min	Max	DV	Parameters	Min	Max	Value
$V_{g1}(p.u.)$	0.95	1.1	1.068	$f_1(MW)$			4.551
$V_{g2}(p.u.)$	0.95	1.1	1.059	$f_2(p.u.)$			0.325
$V_{g5}(p.u.)$	0.95	1.1	1.037	$Q_{G1}(MVAr)$	-20	150	0.886
$V_{g8}(p.u.)$	0.95	1.1	1.038	$Q_{G2}(MVAr)$	-20	60	11.758
$V_{g11}(p.u.)$	0.95	1.1	1.040	$Q_{G5}(MVAr)$	-15	62.5	23.994
$V_{g13}(p.u.)$	0.95	1.1	1.032	$Q_{G8}(MVAr)$	-15	48.7	28.070
$T_{11}(p.u.)$	0.9	1.1	3.401	$Q_{G11}(MVAr)$	-10	40	20.050
$T_{12}(p.u.)$	0.9	1.1	4.424	$Q_{G13}(MVAr)$	-15	44.7	11.052
$T_{15}(p.u.)$	0.9	1.1	3.169				
$T_{36}(p.u.)$	0.9	1.1	4.915				
$Q_{C10}(MVAr)$	0	5	4.235				
$Q_{C12}(MVAr)$	0	5	5.000				
$Q_{C15}(MVAr)$	0	5	3.418				
$Q_{C17}(MVAr)$	0	5	4.995				
$Q_{C20}(MVAr)$	0	5	2.504				
$Q_{C21}(MVAr)$	0	5	1.099				
$Q_{C23}(MVAr)$	0	5	0.940				
$Q_{C24}(MVAr)$	0	5	1.031				
$Q_{C29}(MVAr)$	0	5	0.995				

Table 6. Comparison of the results of case studies for the IEEE 30-bus system.

Algorithm	f_1 (MW)	f_2 (p.u.)
MEAASS [59]	6.8893	3.98230
MODE [2]	4.8300	0.12040
OSAMGSA [62]	5.0713	0.11260
MODEA [63]	5.1582	0.22233
PSO [61]	5.3751	0.36510
NSGAII [60]	6.7052	1.73660
QOTLBO [10]	5.2594	0.12100
CPSMOEA [19]	4.9818	0.37420
QOTLBO [10]	4.4126	0.9029
Proposed	4.5511	0.3251

Table 6 clearly shows that the proposed algorithm competed with most of the MOEAs in the base case. The simulation results of the proposed algorithm dominated the results of MEAASS [59], NSGAII [60], and PSO [61]. The recent advantages of wind and solar integration in power systems provide opportunities for more comprehensive and efficient solutions to ORPD problems, leading to a greener, more reliable, and optimized power system operation. Therefore, in the next section, the IEEE 30-bus network is modified to integrate uncertain wind solar generation.

5.2. Stochastic Multi-Objective ORPD

The IEEE 30-bus was considered to evaluate the proposed algorithm's usefulness in solving stochastic multi-objective ORPD problems. A detailed description of the decision variable and the modified test network is shown in Table 2. Furthermore, the active power of thermal generators was kept fixed in all scenarios, that is, at 75, 25, and 30 MW, whereas the power generated by slack bus generators was computed using the Newton Raphson load flow method. Wind and solar generators are uncertain, and the power generation of these generators depends upon wind velocity and solar irradiances. As discussed in Section 3, the wind generator and photovoltaic system output can vary in different scenarios. Hence, if the active power is low from these renewable sources, the swing generator must compensate and maintain the power balance. In this analysis, the maximum power output of the swing generator was sufficiently high, at 200 MW, to ensure that the generator can compensate for the demand, even if the real power production from renewable sources was low or zero. To show the performance of the proposed algorithm, various study cases of conflicting 2, 3, and 4 objective functions were considered and simultaneously optimized. The proposed study cases of the stochastic multi-objective ORPD problem were:

Case 1: Power loss (f_1) vs. voltage deviation (f_2)
Case 2: Voltage deviation (f_2) vs. cost (f_3)
Case 3: Cost (f_3) vs. emission (f_4) vs. voltage deviation (f_2)
Case 4: Cost (f_3) vs. power loss (f_1) vs. voltage deviation (f_2)
Case 5: Cost (f_3) vs. emission (f_4) vs. power loss (f_1) vs. voltage deviation (f_2)

In the stochastic study, 24 scenarios were generated, as shown in Table 3. All the scenarios were combined to form an islanded network, where the search algorithm found that the feasible decision vector and objective functions were optimized as a single network. Expected values of the objective functions of the cases are provided in Equations (3)–(5) and (7). In this paper, the objective functions of each case's scenarios were simultaneously optimized to compute the expected values of the objective functions. The Pareto front of the expected values for the objective functions of cases 1, 2, 3, and 4, considering all the scenarios, is shown in Figure 7. Figure 7 shows that the proposed algorithm searched the evenly spaced and approximate global optimal solutions in most cases. The data tip in Figure 7 shows the best compromise solution. Compared to the deterministic base case (100% loading), stochastic ORPD yielded a better solution. In the stochastic study, mean loading was 80%, along with the wind and solar integration.

Therefore, the overall performance of the stochastic study seems to be better. In case 1, the expected voltage deviation was 0.1444 p.u. and the expected P_L was 2.47 MW.
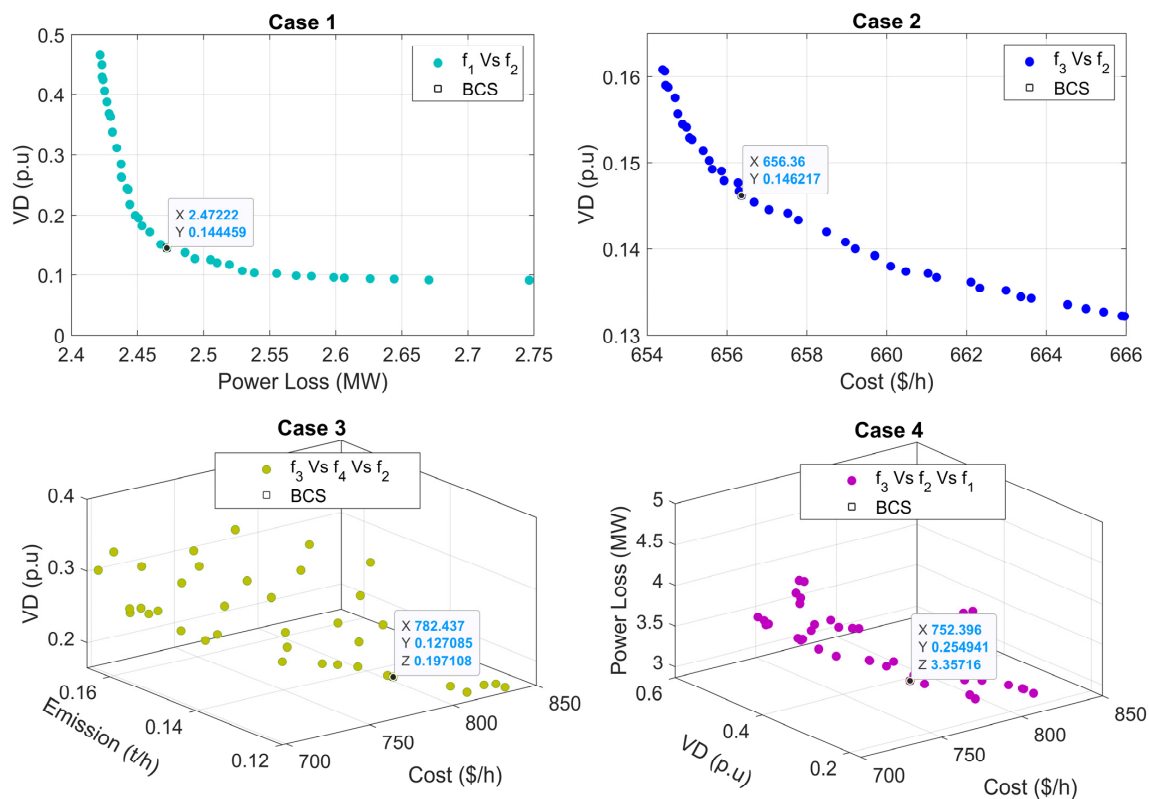

Figure 7. Final non-dominated solutions of cases 1, 2, 3, and 4.

In case 2, the VD was slightly higher compared to case 1, which was 0.14 p.u., and another objective function was the expected cost of active and reactive power generation that was minimized up to 656.36 USD/h. The VD was slightly higher in case 2 because of power loss as the objective function in case 1, emphasizing that power loss minimization was achieved by increasing the voltage level of the system. In case 3, the obtained minimum values of the expected objective functions of cost, emission, and VD were 782.4 (USD/h), 0.127 (t/h), and 0.197 p.u., respectively. In case 4, the final objective functions of cost, VD, and power loss were 752.369 (USD/h), 0.255 p.u., and 3.357 MW, respectively. In case 3, the cost was higher than that in case 4 due to the simultaneous minimization of the VD and power loss in case 4. Considering the VD, one of the objective functions emphasized those solutions that yielded voltage near unity and less reactive power injected by the generators; hence, the cost decreased to some extent. However, the active power of all the thermal generators was fixed, and only the variables wind and solar power were optimized, whereas the slack bus generator was used to balance the generation. Figure 8 shows the results of the final non-dominated solution of case 5; in this case, all the objective functions were optimized to show the proposed algorithm's effectiveness in solving many-objective optimizations. In Figure 8, each vertical line is the objective function, and each horizontal line shows a solution. Figure 5 demonstrates how the suggested approach located the widely dispersed final non-dominated solutions from which the decision-maker can choose one solution. Finally, in all the cases, a fuzzy decision-making technique was employed to select the best compromise solution (BCS). That single BCS of all the cases comprises solutions for all the scenarios.
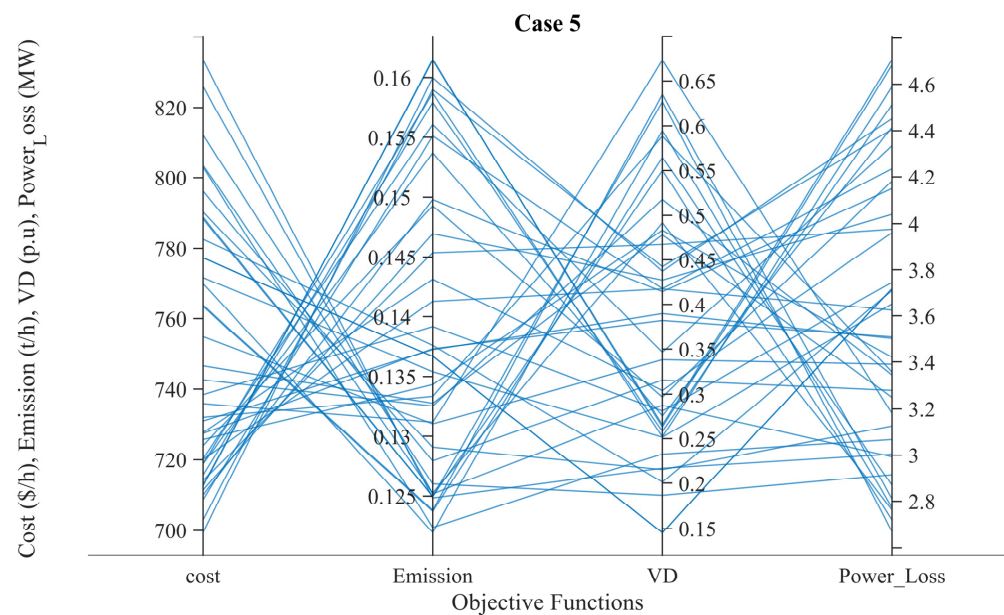
Figure 8. Parallel plot of final non-dominated solutions of case 5.

Table 7 shows the BCSs of all the scenarios shown in Figures 7 and 8. Figure 9a–c show the box plot and the mean value of the PV bus voltage, V_g, and transformer tap ratio, Tap_m. Moreover, reactive power was produced by the conventional thermal generators. Each box in the box plot shows the median, the lower and upper quartiles, and any outliers of all the scenarios of all cases. Statistically, Figure 9a–c show that all the variables were within the upper and lower limits. However, Figure 9d presents the load bus voltage (V_L) of all the scenarios of all cases. Each box plot of all the scenarios has lower and upper limits of 0.95 and 1.05 p.u. Compared to all the cases, the mean value of the load bus voltage profile seems ideal in case 2, which was smooth in all the scenarios and near unity. In all other cases, the mean value of the load bus voltage of all the scenarios highly fluctuated.

Table 7. Simulation results considering the BCSs of all the scenarios of all the cases.

| Case 1		Case 2		Case 3			Case 4			Case 5			
P_L	VD	C	VD	C	E	VD	C	VD	P_L	P_L	VD	C	E
0.3854	0.0169	0.5788	0.0001	76.8483	0.0151	0.0410	45.2758	0.0143	0.1655	0.009	0.001	2.304	0.000
0.0520	0.0025	129.7699	0.0166	98.5414	0.0088	0.0223	0.6817	0.0003	0.0024	0.521	0.062	98.579	0.019
0.0028	0.0008	23.0903	0.0066	11.5296	0.0019	0.0080	0.6660	0.0005	0.0039	0.024	0.004	5.865	0.001
1.1047	0.0565	18.6248	0.0058	47.5168	0.0074	0.0073	5.2365	0.0014	0.0209	0.055	0.003	18.468	0.003
0.0054	0.0005	60.7755	0.0108	2.2249	0.0004	0.0013	22.2890	0.0195	0.1353	0.044	0.005	10.161	0.001
0.0742	0.0054	1.3350	0.0002	12.1470	0.0021	0.0026	0.7403	0.0001	0.0033	0.086	0.004	16.910	0.003
0.1701	0.0097	1.3236	0.0002	15.5695	0.0030	0.0051	0.7936	0.0002	0.0034	0.006	0.000	1.705	0.000
0.0053	0.0006	4.0056	0.0009	2.5370	0.0004	0.0007	10.6897	0.0048	0.0391	0.003	0.000	0.788	0.000
0.0191	0.0025	6.4680	0.0011	4.9001	0.0008	0.0020	13.5671	0.0079	0.0735	0.161	0.014	29.053	0.005
0.0605	0.0054	3.5640	0.0005	13.5063	0.0024	0.0041	2.2948	0.0012	0.0141	0.357	0.017	52.734	0.009
0.0443	0.0054	8.0674	0.0010	7.2406	0.0012	0.0031	66.3879	0.0276	0.3127	0.452	0.049	88.868	0.013
0.0404	0.0033	0.6962	0.0001	1.6501	0.0002	0.0006	11.3310	0.0035	0.0619	0.126	0.007	29.782	0.004
0.1025	0.0046	0.7417	0.0001	4.8896	0.0008	0.0011	76.5913	0.0242	0.3976	0.279	0.014	42.425	0.009
0.0024	0.0005	9.5765	0.0031	2.4825	0.0004	0.0016	0.8257	0.0004	0.0031	0.004	0.000	0.804	0.000
0.1052	0.0084	2.2995	0.0004	5.0162	0.0009	0.0016	0.7368	0.0004	0.0040	0.068	0.003	13.301	0.002
0.0275	0.0020	9.4191	0.0012	26.8187	0.0039	0.0057	2.4149	0.0007	0.0144	0.085	0.012	19.997	0.003
0.0035	0.0005	0.7661	0.0002	298.1198	0.0549	0.0417	1.7304	0.0010	0.0105	0.039	0.003	5.040	0.001
0.0087	0.0016	64.4279	0.0146	10.7845	0.0017	0.0048	324.9457	0.0928	1.1847	0.073	0.004	9.000	0.002
0.0042	0.0002	121.0430	0.0235	0.7877	0.0001	0.0006	120.9879	0.0401	0.6263	0.011	0.001	1.740	0.000
0.0020	0.0002	1.6372	0.0003	19.0488	0.0024	0.0133	0.8647	0.0003	0.0058	2.308	0.154	364.957	0.059
0.0029	0.0002	2.4463	0.0012	0.8557	0.0001	0.0004	9.1820	0.0044	0.0770	0.103	0.011	15.653	0.003
0.0063	0.0008	173.0970	0.0565	40.3325	0.0075	0.0164	10.5969	0.0035	0.0556	0.011	0.001	1.764	0.000
0.2194	0.0139	8.9840	0.0013	4.0063	0.0006	0.0017	5.1802	0.0021	0.0225	0.005	0.000	0.952	0.000
0.0237	0.0019	3.6276	0.0005	75.0836	0.0103	0.0101	18.3862	0.0027	0.1189	0.111	0.003	14.552	0.003
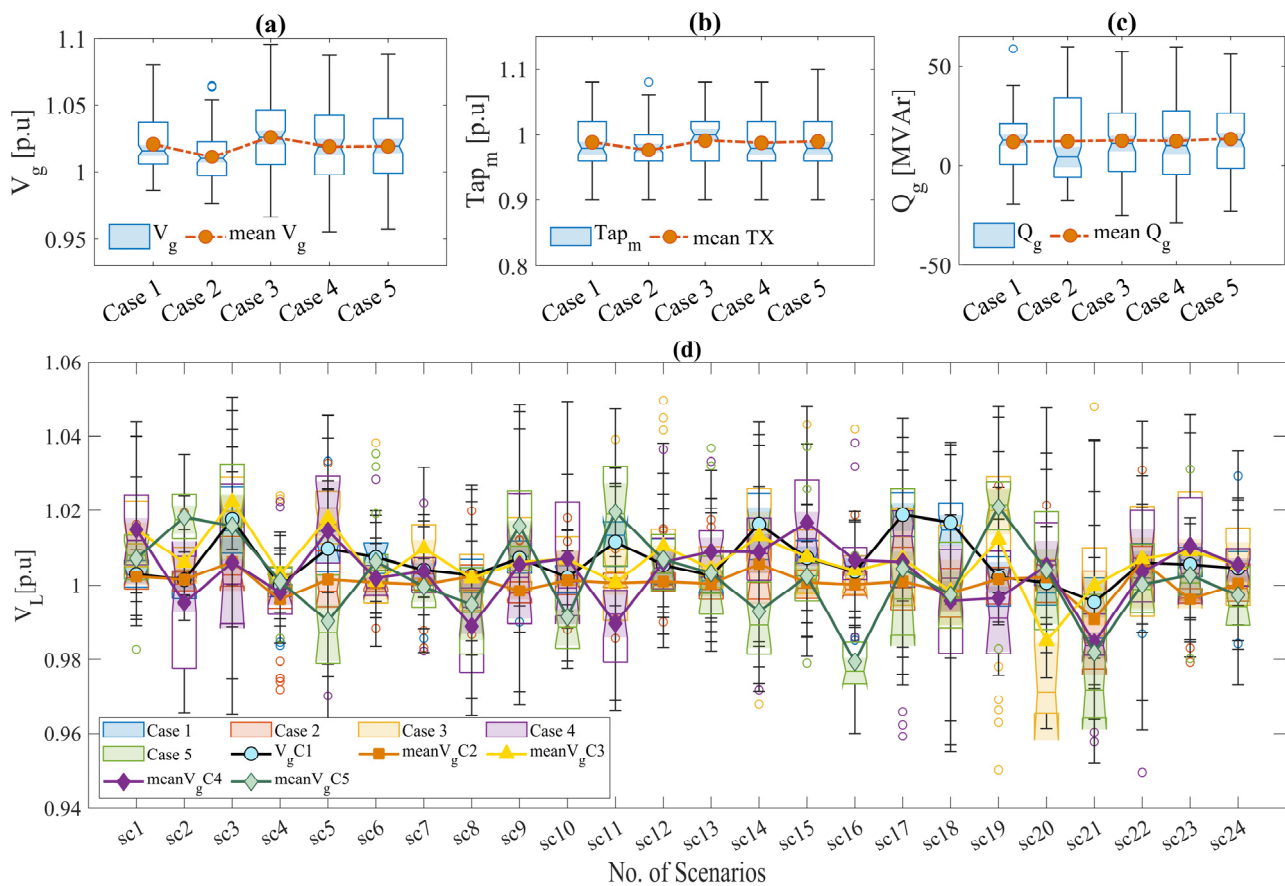
Figure 9. Box plot for (**a**) generator bus voltage V_g (**b**) Transformer tap ratio Tap_m (**c**) MVAr injection of generators Q_g and (**d**) Load bus voltage V_L of all the scenarios of all the cases.

6. Discussion

In the field of power systems' engineering, the multi-objective ORPD problem is a prominent study topic. It entails distributing reactive power among various power system components in order to simultaneously optimize different objectives. Section 1 presented recent ORPD literature and the primary findings and limitations. For the purpose of solving the single- and multi-objective ORPD problems, majority of researchers in the literature used the IEEE 30-bus test system. Therefore, the IEEE 30-bus system was taken into consideration in this research to determine the ORPD problem's solution.

In the past, power loss, VD, and the stability index were often employed to solve ORPD issues. To demonstrate the proposed algorithm's superiority and performance, this research compared it to existing approaches in the literature using classical objective functions. Table 6 shows that, when compared to other approaches described in the literature in terms of the Pareto front (PF) and statistical comparisons, such as maximum, minimum, and standard deviation values, the suggested algorithm approximated the global optimal solution. When compared to all the other algorithms, the obtained value of the HVI was at its highest, at 0.197.

Wind and solar power integration into ORPD has garnered interest in recent decades. Wind and solar electricity have unique properties that make their incorporation into power systems difficult. Recent studies have optimized reactive power allocation by including wind and solar power concerns in ORPD formulations. As a result, the proposed test systems in this study were integrated with technologies for renewable energy sources, such as wind turbines and solar PV units. Moreover, load demand, wind, and solar power generation were modeled using normal, Weibull, and lognormal PDFs. Using the proposed PDFs, 1000 MCS-based scenarios are developed with credibility. The computing cost of

finding solutions for each of these circumstances is high. Then, the 24 typical scenarios shown in Table 3 were discovered using the scenario reduction technique. Additionally, the authors have proposed five MO-RPD instances that seek to optimize a variety of competing objective functions that efficiently distribute reactive power among all devices, while taking into account the influence of unpredictable wind and solar PV generation. The simulation results of all the cases of all the scenarios are shown in Figures 7 and 8, and the BCSs (expected values of the objective functions of all the scenarios) of all the cases are provided in Table 7. The figures clearly showed that the proposed algorithm found the near-global optimal and widely distributed solutions in a single simulation run. Figure 9a–c clearly show that all the decision variables were within the desirable limit, and the overall performance of cases 2 and 3 was better compared to all the other cases in terms of the minimum value of the decision variable. Figure 9d shows a statistical box plot of the voltage levels of all the load buses of all the scenarios. The box plot clearly showed that the voltage levels in all the scenarios were within 0.95 to 1.05 p.u. Cases 1 to 4 comprised of 2 and 3 conflicting objective functions, in the category of multi-objective optimization. It is interesting to note that the proposed algorithm showed well-distributed final non-dominated solutions considering four conflicting objective functions.

Optimizing multiple objectives can become increasingly complex as the number of objectives increases, such as in case 5 in our study. The use of many-objective optimization evolutionary algorithms (MaOEAs) is indeed a relevant approach to effectively address this challenge. In the literature, the problem of case 5 is called the many-objective optimization problems (MaOPs), and recently designed MaOEAs are implemented to find the optimal solutions of mathematical benchmark functions of MaOPs, such as NSGAIII [37], KnEA [38], and IDBEA [39]. These algorithms are specifically designed to handle a large number of objectives (especially more than three) and can provide more robust solutions in such cases. In this paper, all the above-discussed MaOEAs were implemented to find the optimal solution for the case 5 MOORPD problem. Figure 10 shows a comparison of the proposed algorithm with the recently implemented MaOEAs.
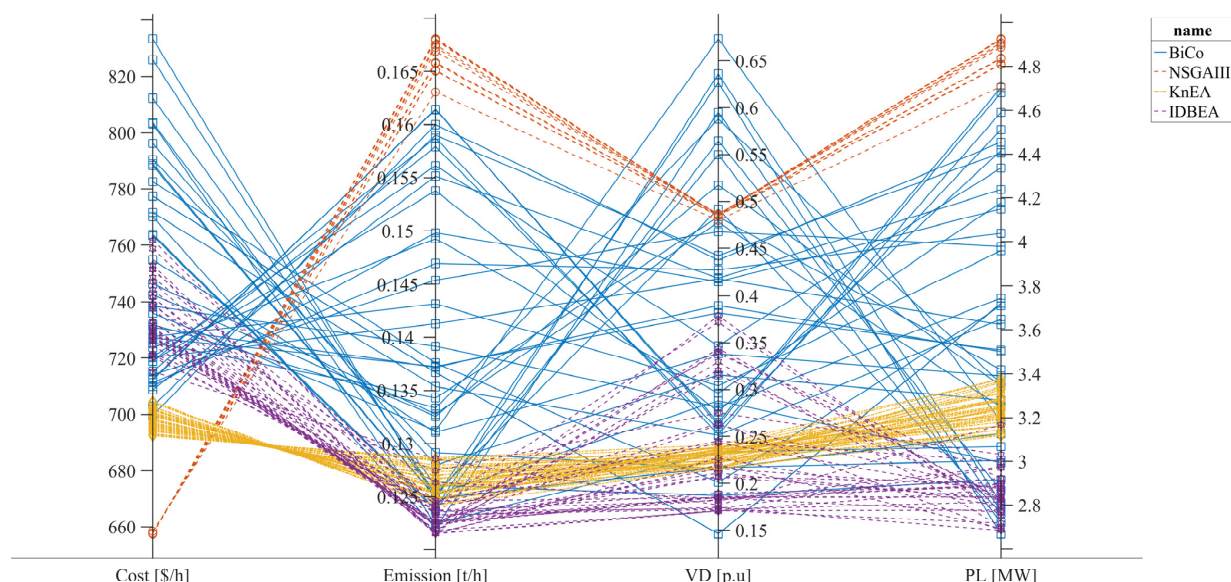

Figure 10. Comparison of the final non-dominated solutions of the proposed algorithm and other algorithms.

Figure 10 clearly shows that the proposed algorithm found better widely distributed, non-dominated solutions in all the objective functions, compared to the other state-of-the-art MaOEAs. NSGAIII emphasized the first objective function, whereas, in the other objective functions, NSGAIII became stuck in the local optimal region. The simulation results of IDBEA are promising compared to the NSGAIII and KnEA algorithms. Through

the application of these five cases, we have demonstrated the effectiveness of our proposed approach in achieving optimal reactive power allocation and addressing the multiple objectives of power loss minimization, voltage deviation, the cost of reactive power generation, and the emission rate. The simulation results obtained from all the cases indicated significant improvements in the system performance and validated the efficacy of our proposed methodologies. The introduction of the proposed algorithm for ORPD provides a comprehensive approach to address the challenges associated with reactive power allocation in power systems.

7. Conclusions

In this paper, two studies, deterministic and stochastic, were considered to solve the multi-objective ORPD problem. Firstly, the deterministic multi-objective ORPD problem was considered using the most popular objective functions, such as power loss and the VD. This study aimed to show the superiority and performance of the proposed algorithm with the recently designed MOEAs already implemented in the literature to solve the ORPD problem. The deterministic case simulation results showed that the proposed algorithm found better evenly spaced and approximate global optimal solutions compared to other recently designed MOEAs. Each algorithm was run twenty times, independently, for a fair comparison between the various MOEAs. Statistical parameters of all twenty runs (best, worst, and standard deviation values), based on the hypervolume indicators (HVI) and inverse geometric distance (IGD) metrics, popularly used performance metrics, were considered. The proposed algorithm found better results regarding the HVI and IGD than most of the implemented MOEAs.

A real large-scale stochastic multi-objective ORPD problem was formulated using a modified IEEE 30-bus test system. In the stochastic study, variability in load demand, wind, and solar PV units was computed using suitable mathematical models, such as normal, Weibull, and lognormal probability density functions (PDFs). In the stochastic ORPD problem, 1000 MCS-based random scenarios were initially generated using the PDFs; then, the scenario reduction technique was applied to reduce the size of the problem. Table 2 shows the size of the modified IEEE 30-bus test system. Various study cases comprised of 2, 3, and 4 conflicting objective functions were considered to show the superiority of the proposed algorithm. Pareto fronts of stochastic cases in the simulation results section clearly showed that the proposed method can find the approximate global non-dominated solution of 2, 3, and 4 conflicting objective functions for the decision-maker. Finally, the fuzzy weighted factor was applied to find the final non-dominated solutions.

8. Future Work

In the future, proposed formulations can be extended to implement reactive power reserves, fixed zonal reserves, or contingency studies considering many-objective optimization problems. Furthermore, recently implemented MaOEAs are unconstrained; therefore, effective constraint-handling techniques can be integrated to enhance the capability and performance of MaOEAs to solve many-objective ORPD problems.

Author Contributions: All authors planned the study and contributed to the idea and field of information. All authors have read and agreed to the published version of the manuscript.

Nomenclature

Symbol

BCS	Best compromise solution	N_W	Total number of wind generators
BiCo	Bidirectional co-evolutionary	N_S	Total number of solar PV units
CHT	Constraint-handling technique	N_{SVC}	Total number of shunt VAR compensators
DV	Decision vector	N_{TX}	Total number of transformers
MCS	Monte Carlo simulation	N_{pq}	Total number of load or PQ buses
MOP	Multi-objective optimization problem	N_g	Total number of generators (thermal, wind, and solar PV)
MaOP	Many-objective optimization problem		
MOEA	Multi-objective evolutionary algorithm	n_{sc}	Total number of scenarios
MaOEA	Many-objective evolutionary algorithm	nl	Total number of lines
ORPD	Optimal reactive power dispatch	P_G, P_D	Active power generation and demand
PDF	Probability density functions	P_L	Power loss (MW)
PF	Pareto front	P_{gT}, Q_{gT}	Active and reactive power of thermal genera
SVC	Shunt VAR compensator	P_{gW}, P_{gS}	Active power of wind and solar PV unit
SD	Standard deviation	Q_c	Vector of SVC
TX	Transformers	Q_G, Q_D	Reactive power generation and demand
VD	Voltage deviation	S	Feasible search space
		sc	Current scenarios
		S_l^{max}, S_l	Maximum and actual MVA flow limit in the lth branch
		T	Transpose of vector

Variable and Parameter Indexing

a, b, c	Quadratic cost parameters of thermal unit	Tap_m	Vector of transformer tap settings
$\alpha, \beta, \gamma, \omega, \mu$	Emission coefficients of thermal unit	V_i, V_j	The voltage from and to the bus
α, β	Scale and shape parameters of Weibull PDF	V_G	Vector of voltage set point of all the generators
B_{ij}	Shunt susceptance of line between bus i and j	V_L, V_g	The voltage at PQ and PV buses
$C(\bullet)$	Total cost of active and reactive generation	x	Decision vector
C_j and C_k	Cost parameters of wind and solar PV units	τ_{sc}	Probability of scenario sc
D	Total number of the decision variable	δ_{ij}	Branch angle between bus i and j
E	Emission (t/h)	$\Delta_D, \Delta_v, \Delta_G$	PDFs of percentage load, wind velocity, and solar irradiances
$F(x)$	Vector of multi-objective function	v_w, G_S	Wind velocity and solar irradiance
G_k	Shunt conductance of the kth line	μ_d, σ_d	Mean and SD of normal PDF
g, h	Number of p and q vectors of equality and inequality constraints	μ_s, σ_s	Mean and SD of lognormal PDF
i, j	From and to bus		
N_b	Total number of buses		
N_T	Total number of thermal generators		

References

1. Ali, M.H.; Soliman, A.M.A.; Abdeen, M.; Kandil, T.; Abdelaziz, A.Y.; El-Shahat, A. A Novel Stochastic Optimizer Solving Optimal Reactive Power Dispatch Problem Considering Renewable Energy Resources. *Energies* **2023**, *16*, 1562. [CrossRef]
2. Shojaei, A.H.; Ghadimi, A.A.; Miveh, M.R.; Mohammadi, F.; Jurado, F. Multi-objective optimal reactive power planning under load demand and wind power generation uncertainties using ε-constraint method. *Appl. Sci.* **2020**, *10*, 2859. [CrossRef]
3. Gupta, S.K.; Kumar, L.; Kar, M.K.; Kumar, S. Optimal reactive power dispatch under coordinated active and reactive load variations using FACTS devices. *Int. J. Syst. Assur. Eng. Manag.* **2022**, *13*, 2672–2682. [CrossRef]
4. Jie, Z.; Shengchun, L.; Yao, R.; Liang, D.; Zhanshan, Y.; Yongfei, M. Reactive power optimization for AVC system based on decoupled interior point method. In Proceedings of the 2022 14th International Conference on Measuring Technology and Mechatronics Automation (ICMTMA), Changsha, China, 15–16 January 2022; pp. 131–133.
5. Grudinin, N. Reactive power optimization using successive quadratic programming method. *IEEE Trans. Power Syst.* **1998**, *13*, 1219–1225. [CrossRef]
6. Kar, M.K.; Kumar, S.; Singh, A.K.; Panigrahi, S. Reactive power management by using a modified differential evolution algorithm. *Optim. Control Appl. Methods* **2023**, *44*, 967–986. [CrossRef]
7. Shaw, B.; Mukherjee, V.; Ghoshal, S.P. Solution of reactive power dispatch of power systems by an opposition-based gravitational search algorithm. *Int. J. Electr. Power Energy Syst.* **2014**, *55*, 29–40. [CrossRef]
8. Pg, A.K.; Devaraj, D. Hybrid CAC-DE in optimal reactive power dispatch (ORPD) for renewable energy cost reduction. *Sustain. Comput. Inform. Syst.* **2022**, *35*, 100688. [CrossRef]
9. Basu, M. Quasi-oppositional differential evolution for optimal reactive power dispatch. *Int. J. Electr. Power Energy Syst.* **2016**, *78*, 29–40. [CrossRef]
10. Mandal, B.; Roy, P.K. Optimal reactive power dispatch using quasi-oppositional teaching learning based optimization. *Int. J. Electr. Power Energy Syst.* **2013**, *53*, 123–134. [CrossRef]
11. Ng Shin Mei, R.; Sulaiman, M.H.; Mustaffa, Z.; Daniyal, H. Optimal reactive power dispatch solution by loss minimization using moth-flame optimization technique. *Appl. Soft Comput.* **2017**, *59*, 210–222. [CrossRef]
12. Chen, G.; Liu, L.; Zhang, Z.; Huang, S. Optimal reactive power dispatch by improved GSA-based algorithm with the novel strategies to handle constraints. *Appl. Soft Comput.* **2017**, *50*, 58–70. [CrossRef]
13. Mehdinejad, M.; Mohammadi-Ivatloo, B.; Dadashzadeh-Bonab, R.; Zare, K. Solution of optimal reactive power dispatch of power systems using hybrid particle swarm optimization and imperialist competitive algorithms. *Int. J. Electr. Power Energy Syst.* **2016**, *83*, 104–116. [CrossRef]

14. Rajan, A.; Malakar, T. Optimal reactive power dispatch using hybrid Nelder–Mead simplex based firefly algorithm. *Int. J. Electr. Power Energy Syst.* **2015**, *66*, 9–24. [CrossRef]

15. Ghasemi, M.; Ghavidel, S.; Ghanbarian, M.M.; Habibi, A. A new hybrid algorithm for optimal reactive power dispatch problem with discrete and continuous control variables. *Appl. Soft. Comput.* **2014**, *22*, 126–140. [CrossRef]

16. Zhihuan, L.; Yinhong, L.; Xianzhong, D. Non-dominated sorting genetic algorithm-II for robust multi-objective optimal reactive power dispatch. In *IET Generation, Transmission & Distribution*; Institution of Engineering and Technology: Hong Kong, China, 2010; Volume 4, pp. 1000–1008.

17. Ramesh, S.; Kannan, S.; Baskar, S. An improved generalized differential evolution algorithm for multi-objective reactive power dispatch. *Eng. Optim.* **2012**, *44*, 391–405. [CrossRef]

18. Nuaekaew, K.; Artrit, P.; Pholdee, N.; Bureerat, S. Optimal reactive power dispatch problem using a two-archive multi-objective grey wolf optimizer. *Expert Syst. Appl.* **2017**, *87*, 79–89. [CrossRef]

19. Zhang, M.; Li, Y. Multi-Objective Optimal Reactive Power Dispatch of Power Systems by Combining Classification-Based Multi-Objective Evolutionary Algorithm and Integrated Decision Making. *IEEE Access* **2020**, *8*, 38198–38209. [CrossRef]

20. Jeyadevi, S.; Baskar, S.; Babulal, C.K.; Willjuice Iruthayarajan, M. Solving multiobjective optimal reactive power dispatch using modified NSGA-II. *Int. J. Electr. Power Energy Syst.* **2011**, *33*, 219–228. [CrossRef]

21. Saraswat, A.; Saini, A. Multi-objective optimal reactive power dispatch considering voltage stability in power systems using HFMOEA. *Eng. Appl. Artif. Intell.* **2013**, *26*, 390–404. [CrossRef]

22. Chen, G.; Liu, L.; Song, P.; Du, Y. Chaotic improved PSO-based multi-objective optimization for minimization of power losses and L index in power systems. *Energy Convers. Manag.* **2014**, *86*, 548–560. [CrossRef]

23. Preetha Roselyn, J.; Devaraj, D.; Dash, S.S. Multi Objective Differential Evolution approach for voltage stability constrained reactive power planning problem. *Int. J. Electr. Power Energy Syst.* **2014**, *59*, 155–165. [CrossRef]

24. Ghasemi, A.; Valipour, K.; Tohidi, A. Multi objective optimal reactive power dispatch using a new multi objective strategy. *Int. J. Electr. Power Energy Syst.* **2014**, *57*, 318–334. [CrossRef]

25. Mouassa, S.; Bouktir, T. Multi-objective ant lion optimization algorithm to solve large-scale multi-objective optimal reactive power dispatch problem. *COMPEL* **2019**, *38*, 304–324. [CrossRef]

26. Chen, G.; Cao, J.; Zhang, Z.; Sun, Z. Application of imperialist competitive algorithm with its enhanced approaches for multi-objective optimal reactive power dispatch problem. *Eng. Lett.* **2019**, *27*, 579–592.

27. Zhou, B.; Chan, K.W.; Yu, T.; Wei, H.; Tang, J. Strength Pareto Multigroup Search Optimizer for Multiobjective Optimal Reactive Power Dispatch. *IEEE Trans. Ind. Inf.* **2014**, *10*, 1012–1022. [CrossRef]

28. Mohseni-Bonab, S.M.; Rabiee, A. Optimal reactive power dispatch: A review, and a new stochastic voltage stability constrained multi-objective model at the presence of uncertain wind power generation. In *IET Generation, Transmission & Distribution*; Institution of Engineering and Technology: Hong Kong, China, 2017; Volume 11, pp. 815–829.

29. Mohseni-Bonab, S.M.; Rabiee, A.; Mohammadi-Ivatloo, B. Voltage stability constrained multi-objective optimal reactive power dispatch under load and wind power uncertainties: A stochastic approach. *Renew. Energy* **2016**, *85*, 598–609. [CrossRef]

30. Aljohani, T.M.; Ebrahim, A.F.; Mohammed, O. Single and multiobjective optimal reactive power dispatch based on hybrid artificial physics–particle swarm optimization. *Energies* **2019**, *12*, 2333. [CrossRef]

31. Keerio, M.U.; Ali, A.; Saleem, M.; Hussain, N.; Hussain, R. Multi-Objective Optimal Reactive Power Dispatch Considering Probabilistic Load Demand Along with Wind and Solar Power Integration. In Proceedings of the 2020 2nd International Conference on Smart Power & Internet Energy Systems (SPIES), Bangkok, Thailand, 15–18 September 2020; pp. 502–507.

32. Etghani, M.M.; Shojaeefard, M.H.; Khalkhali, A.; Akbari, M. A hybrid method of modified NSGA-II and TOPSIS to optimize performance and emissions of a diesel engine using biodiesel. *Appl. Eng.* **2013**, *59*, 309–315. [CrossRef]

33. Liang, R.-H.; Wang, J.-C.; Chen, Y.-T.; Tseng, W.-T. An enhanced firefly algorithm to multi-objective optimal active/reactive power dispatch with uncertainties consideration. *Int. J. Electr. Power Energy Syst.* **2015**, *64*, 1088–1097. [CrossRef]

34. Wu, Z.; Zhuang, Y.; Zhou, S.; Xu, S.; Yu, P.; Du, J.; Luo, X.; Abbas, G. Bi-Level Planning of Multi-Functional Vehicle Charging Stations Considering Land Use Types. *Energies* **2020**, *13*, 1283. [CrossRef]

35. Alkayem, N.F.; Parida, B.; Pal, S. Optimization of friction stir welding process using NSGA-II and DEMO. *Neural Comput. Appl.* **2019**, *31*, 947–956. [CrossRef]

36. Mohseni-Bonab, S.M.; Rabiee, A.; Mohammadi-Ivatloo, B.; Jalilzadeh, S.; Nojavan, S. A two-point estimate method for uncertainty modeling in multi-objective optimal reactive power dispatch problem. *Int. J. Electr. Power Energy Syst.* **2016**, *75*, 194–204. [CrossRef]

37. Jain, H.; Deb, K. An Evolutionary Many-Objective Optimization Algorithm Using Reference-Point Based Nondominated Sorting Approach, Part II: Handling Constraints and Extending to an Adaptive Approach. *IEEE Trans. Evol. Comput.* **2014**, *18*, 602–622. [CrossRef]

38. Ali, A.; Abbas, G.; Keerio, M.U.; Koondhar, M.A.; Chandni, K.; Mirsaeidi, S. Solution of Constrained mixed-integer multi-objective optimal power flow problem considering the hybrid multi-objective evolutionary algorithm. *IET Gener. Transm. Distrib.* **2023**, *17*, 66–90. [CrossRef]

39. Asafuddoula, M.; Ray, T.; Sarker, R. A Decomposition-Based Evolutionary Algorithm for Many Objective Optimization. *IEEE Trans. Evol. Comput.* **2015**, *19*, 445–460. [CrossRef]

40. Sun, Y.; Yen, G.G.; Yi, Z. IGD Indicator-Based Evolutionary Algorithm for Many-Objective Optimization Problems. *IEEE Trans. Evol. Comput.* **2019**, *23*, 173–187. [CrossRef]
41. Sun, Y.; Xue, B.; Zhang, M.; Yen, G.G. A New Two-Stage Evolutionary Algorithm for Many-Objective Optimization. *IEEE Trans. Evol. Comput.* **2019**, *23*, 748–761. [CrossRef]
42. He, Z.; Yen, G.G. Many-Objective Evolutionary Algorithm: Objective Space Reduction and Diversity Improvement. *IEEE Trans. Evol. Comput.* **2016**, *20*, 145–160. [CrossRef]
43. Granados, J.F.L.; Uturbey, W.; Valadão, R.L.; Vasconcelos, J.A. Many-objective optimization of real and reactive power dispatch problems. *Int. J. Electr. Power Energy Syst.* **2023**, *146*, 108725. [CrossRef]
44. Biswas, P.P.; Suganthan, P.N.; Qu, B.Y.; Amaratunga, G.A.J. Multiobjective economic-environmental power dispatch with stochastic wind-solar-small hydro power. *Energy* **2018**, *150*, 1039–1057. [CrossRef]
45. Deb, K.; Pratap, A.; Agarwal, S.; Meyarivan, T. A fast and elitist multiobjective genetic algorithm: NSGA-II. *IEEE Trans. Evol. Comput.* **2002**, *6*, 182–197. [CrossRef]
46. Abbas, G.; Ali, B.; Chandni, K.; Koondhar, M.A.; Chandio, S.; Mirsaeidi, S. A Parametric Approach to Compare the Wind Potential of Sanghar and Gwadar Wind Sites. *IEEE Access* **2022**, *10*, 110889–110904. [CrossRef]
47. Chang, T.P. Investigation on Frequency Distribution of Global Radiation Using Different Probability Density Functions. *Int. J. Appl. Sci. Eng.* **2010**, *8*, 99–107. [CrossRef]
48. Biswas, P.; Suganthan, P.N.; Mallipeddi, R.; Amaratunga, G. Optimal reactive power dispatch with uncertainties in load demand and renewable energy sources adopting scenario-based approach. *Appl. Soft Comput.* **2018**, *75*, 616–632. [CrossRef]
49. Growe-Kuska, N.; Heitsch, H.; Romisch, W. Scenario reduction and scenario tree construction for power management problems. In Proceedings of the 2003 IEEE Bologna Power Tech Conference Proceedings, Bologna, Italy, 23–26 June 2003; Volume 3, p. 7.
50. Liu, Z.Z.; Wang, B.C.; Tang, K. Handling Constrained Multiobjective Optimization Problems via Bidirectional Coevolution. *IEEE Trans. Cybern.* **2022**, *52*, 10163–10176. [CrossRef] [PubMed]
51. Deb, K.; Sindhya, K.; Okabe, T. Self-adaptive simulated binary crossover for real-parameter optimization. In Proceedings of the 9th Annual Conference on Genetic and Evolutionary Computation, London, UK, 7–11 July 2007; pp. 1187–1194. [CrossRef]
52. Habib, S.; Abbas, G.; Jumani, T.A.; Bhutto, A.A.; Mirsaeidi, S.; Ahmed, E.M. Improved Whale Optimization Algorithm for Transient Response, Robustness, and Stability Enhancement of an Automatic Voltage Regulator System. *Energies* **2022**, *15*, 5037. [CrossRef]
53. Liu, Z.; Wang, Y. Handling Constrained Multiobjective Optimization Problems with Constraints in Both the Decision and Objective Spaces. *IEEE Trans. Evol. Comput.* **2019**, *23*, 870–884. [CrossRef]
54. Tian, Y.; Zhang, T.; Xiao, J.; Zhang, X.; Jin, Y. A coevolutionary framework for constrained multiobjective optimization problems. *IEEE Trans. Evol. Comput.* **2020**, *25*, 102–116. [CrossRef]
55. Sun, R.; Zou, J.; Liu, Y.; Yang, S.; Zheng, J. A Multi-stage Algorithm for Solving Multi-objective Optimization Problems with Multi-constraints. *IEEE Trans. Evol. Comput.* **2022**. [CrossRef]
56. Ming, F.; Gong, W.; Wang, L.; Gao, L. A Constrained Many-Objective Optimization Evolutionary Algorithm With Enhanced Mating and Environmental Selections. *IEEE Trans. Cybern.* **2022**. [CrossRef]
57. Ming, F.; Gong, W.; Li, D.; Wang, L.; Gao, L. A Competitive and Cooperative Swarm Optimizer for Constrained Multi-objective Optimization Problems. *IEEE Trans. Evol. Comput.* **2022**. [CrossRef]
58. Tian, Y.; Zhu, W.; Zhang, X.; Jin, Y. A practical tutorial on solving optimization problems via PlatEMO. *Neurocomputing* **2023**, *518*, 190–205. [CrossRef]
59. Hongxin, L.; Yinhong, L.; Jinfu, C. Adaptive multiple evolutionary algorithms search for multi-objective optimal reactive power dispatch. *Int. Trans. Electr. Energy Syst.* **2014**, *24*, 780–795. [CrossRef]
60. Ali, A.; Abbas, G.; Keerio, M.U.; Mirsaeidi, S.; Alshahr, S.; Alshahir, A. Pareto Front-Based Multiobjective Optimization of Distributed Generation Considering the Effect of Voltage Dependent Nonlinear Load Models. *IEEE Access* **2023**, *11*, 12195–12217. [CrossRef]
61. Mancer, N.; Mahdad, B.; Srairi, K. Multi objective optimal reactive power flow based STATCOM using three variant of PSO. *Int. J. Energy Eng.* **2012**, *2*, 1–7. [CrossRef]
62. Niknam, T.; Narimani, M.R.; Azizipanah-Abarghooee, R.; Bahmani-Firouzi, B. Multiobjective optimal reactive power dispatch and voltage control: A new opposition-based self-adaptive modified gravitational search algorithm. *IEEE Syst. J.* **2013**, *7*, 742–753. [CrossRef]
63. Nayaka, M.; Rayb, R.; Routc, P. Multi-objective Optimal Reactive Power Dispatch in Power System using Differential Evolution Algorithm. In Proceedings of the International Conference on Emerging Trends in Electrical, Communication and Information Technologies, Anantapur, Andhra Pradesh, India, 21–23 December 2012; pp. 16–26.